Structure
Article

Unique Structural, Dynamical, and Functional Properties of K11-Linked Polyubiquitin Chains

Carlos A. Castañeda,[1] Tanuja R. Kashyap,[1] Mark A. Nakasone,[1] Susan Krueger,[2] and David Fushman[1,*]
[1]Department of Chemistry and Biochemistry, Center for Biomolecular Structure and Organization, University of Maryland, College Park, MD 20742, USA
[2]NIST Center for Neutron Research, National Institute of Standards and Technology, Gaithersburg, MD 20899, USA
*Correspondence: fushman@umd.edu
http://dx.doi.org/10.1016/j.str.2013.04.029

SUMMARY

K11-linked polyubiquitin chains play important signaling and regulatory roles in both degradative and nonproteolytic pathways in eukaryotes. To understand the structural basis of how these chains are recognized and distinguished from other polyubiquitins, we determined solution structures of K11-linked diubiquitin (K11-Ub_2) in the absence and presence of salt. These structures reveal that K11-Ub_2 adopts conformations distinct from those of K48-linked or K63-linked chains. Importantly, our solution NMR and SANS data are inconsistent with published crystal structures of K11-Ub_2. We found that increasing salt concentration compacts K11-Ub_2 and strengthens interactions between the two Ub units. Binding studies indicate that K11-Ub_2 interacts with ubiquitin-receptor proteins from both proteasomal and nonproteasomal pathways but with intermediate affinity and different binding modes than either K48-linked or K63-linked diubiquitin. Our data support the hypothesis that polyubiquitin chains of different linkages possess unique conformational and dynamical properties, allowing them to be recognized differently by downstream receptor proteins.

INTRODUCTION

Ubiquitin (Ub) is a small, highly conserved 8.5 kDa protein that is critical for many cellular signaling pathways in eukaryotes (Fushman and Wilkinson, 2011). Posttranslational modification of proteins via mono- or polyubiquitination signals proteasomal degradation, DNA repair, and cell cycle regulation, among others. The diversity in Ub signaling stems from the ability of Ub to form polyubiquitin (polyUb) chains through covalent linkage between the εNH_2 group of a specific lysine (K6, K11, K27, K29, K33, K48, or K63) or αNH_2 of M1 on one Ub and the C terminus of a second Ub. The focus has been directed recently on elucidating the biological roles of K11-linked polyUb chains (Bremm and Komander, 2011; Wickliffe et al., 2011a). Quantitative mass spectrometry studies determined that K11 linkages could be as abundant as the "canonical" K48 linkages in yeast (Xu et al., 2009). K11 linkages are upregulated during anaphase of the mitotic cycle (Bremm and Komander, 2011; Matsumoto et al., 2010; Wickliffe et al., 2011a). APC/C, an E3 ligase, ubiquitinates mitotic regulatory proteins with K11-linked polyUb chains and directs these proteins for proteasomal degradation during mitotic exit (Williamson et al., 2009). K11 linkages are also involved in endoplasmic reticulum-associated degradation (Xu et al., 2009). Adding to K11's signal versatility, K11-linked chains have been implicated in nondegradative (cytokine signaling, NFκB activation) cellular signaling pathways (Bremm and Komander, 2011; Dynek et al., 2010; Iwai, 2012; Wickliffe et al., 2011a). To understand the role of K11-linked Ub chains in vivo, it is absolutely necessary to elucidate their structural, dynamical, and functional properties in solution.

Recent advances have been made in elucidating the structural biology of K11-linked chains (Bremm et al., 2010; Matsumoto et al., 2010; Wickliffe et al., 2011b), facilitated by the discovery of K11-specific Ub-conjugating E2 enzymes, specifically UbcH10, an initiator E2, and Ube2S, the primary elongator of K11-linked Ub chains (Williamson et al., 2009). Two crystal structures of free unanchored K11-linked Ub_2 (K11-Ub_2) have been published (Bremm et al., 2010; Matsumoto et al., 2010). Remarkably, the Ub/Ub orientations in these two structures are very different from each other. Even more intriguing from a functional standpoint is that the receptor-binding hydrophobic surface patches of the two Ubs in K11-Ub_2 are either adjacent to each other in one structure (Protein Data Bank [PDB] ID 3NOB) (Matsumoto et al., 2010), or facing outward and away from each other in the other structure (PDB ID 2XEW) (Bremm et al., 2010). The differences between the crystal structures raise the question of which of these structures, if any, represents the physiologically relevant conformation of K11-Ub_2. This motivated us to study K11-linked chains in solution under near physiological conditions.

Here we present solution structures and dynamics information of K11-linked chains at neutral pH in the absence and presence of salt. These structures were determined using nuclear magnetic resonance (NMR) spectroscopy and corroborated with small-angle neutron scattering (SANS). Importantly, the NMR and SANS data are inconsistent with the crystal structures of K11-Ub_2 or their motionally averaged combination. We show that K11-linked Ub chains interact with Ub-receptors associated with proteasomal and nonproteasomal pathways differently from K48-linked or K63-linked chains. Our results support the hypothesis that polyUb chains of different linkages code for different signals via unique conformational properties and binding modes to target receptor proteins.

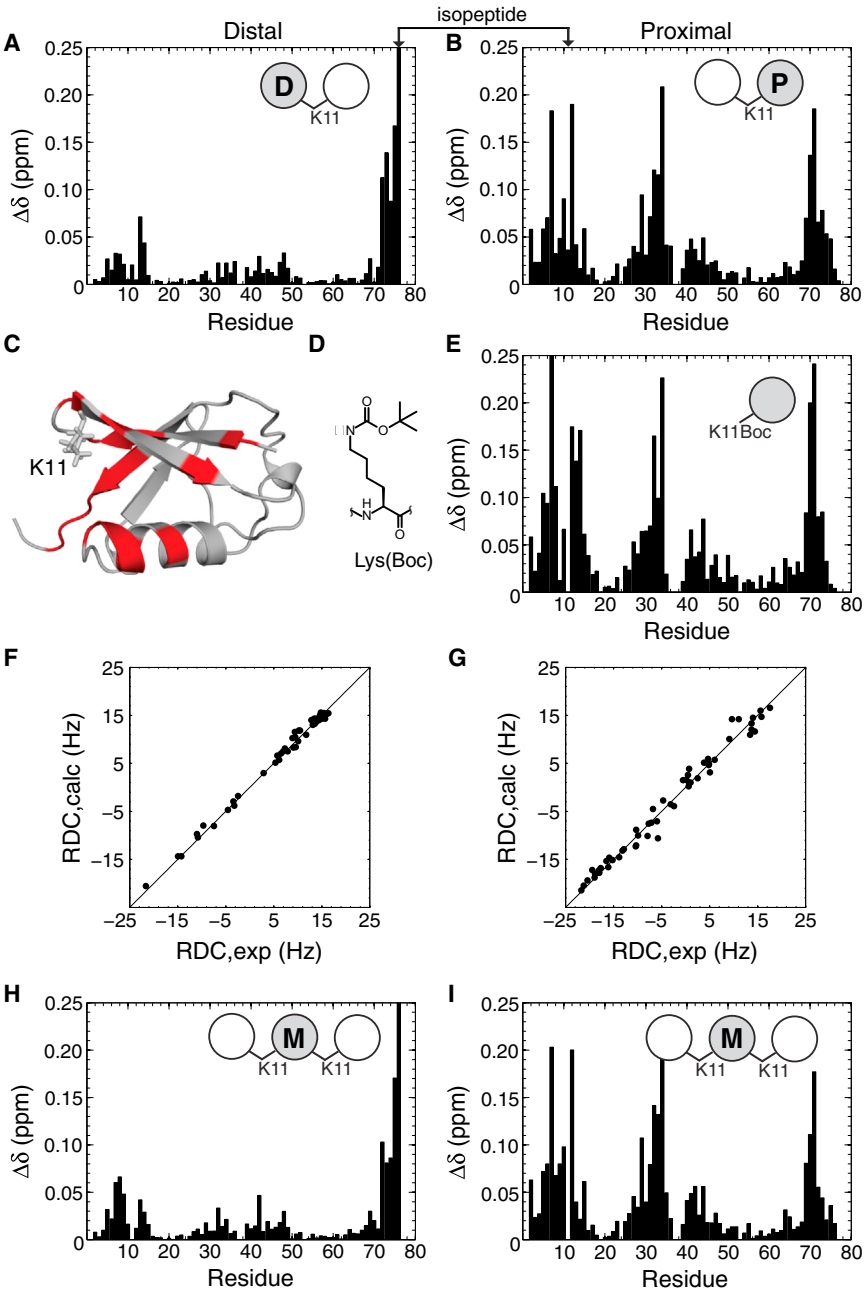

Figure 1. NMR Characterization of K11-Linked Ub Chains

(A and B) Amide chemical shift perturbations (CSPs) of highlighted Ub units in K11-Ub_2 versus their respective Ub monomers.

(C) Proximal-Ub residues with CSPs > 0.05 ppm (red) mapped on Ub structure.

(D) Structure of Lys(Boc).

(E) CSPs in monomeric Ub resulting from K11 to K11Boc mutation.

(F and G) Agreement between experimental and back-calculated RDCs for the distal (F) and proximal (G) Ubs of K11-Ub_2. Atom coordinates from the solution structure of Ub (PDB ID 1D3Z) were used. The solid line represents absolute agreement.

(H and I) CSPs of the middle Ub in all-natural K11-Ub_3 versus the proximal (H) or the distal (I) Ub in all-natural K11-Ub_2.

See also Figure S1.

otherwise known as chemical shift perturbations (CSPs), between each Ub unit in K11-Ub_2 and its respective monomer are quantified in Figures 1A and 1B. The distal Ub showed small but regiospecific CSPs in and around the "canonical" hydrophobic surface patch, comprised of residues L8, I44, and V70 (Beal et al., 1996). The largest perturbations were localized to the C terminus, which is covalently attached to K11 of the proximal Ub via an isopeptide linkage. In contrast to the distal Ub, there are a significant number of CSPs > 0.05 ppm in the proximal Ub; most of these spatially cluster around K11 (Figure 1C). Generally, CSPs indicate a change in the electronic environment of the nucleus under observation and could arise from chemical modification, interprotein interactions, or both. The fact that the CSPs cluster around K11 points to the former. However, a prior study (Bremm et al., 2010) speculated that the large CSPs in the proximal Ub were indicative of a novel Ub/Ub interface for K11-Ub_2 that includes residues clustered around K11 on the proximal Ub and nonhydrophobic sites on the distal Ub. To clarify this issue, we used Lys(Boc) (Figure 1D) as a Lys modification mimicking an isopeptide bond. We observed a near-identical CSP pattern (to that of the proximal Ub) in a monoUb variant, where K11 was mutated to Lys(Boc) (Figure 1E). Therefore, we conclude that the large CSPs observed in the proximal Ub did not arise from its noncovalent interactions with the distal Ub but rather from the isopeptide bond at the K11 side chain. These observations illustrate the care necessary in interpreting CSPs on a structural level.

In order to verify that the chain-terminating mutations had no effect on the properties of K11-linked chains, we constructed K11-Ub_2 and K11-Ub_3 free of any mutations, using

RESULTS

K11-Ub_2 was assembled in the presence of Ub-activating E1 enzyme and Ub-conjugating, K11-specific E2 enzyme, Ube2S (Williamson et al., 2009), using recombinant Ubs with chain-terminating mutations (Pickart and Raasi, 2005). This allowed selective isotope labeling of either Ub unit in Ub_2 for NMR studies (Varadan et al., 2002).

Solution NMR Characterization of K11-Linked Chains

^1H-^{15}N TROSY-HSQC spectra of each Ub unit in K11-Ub_2 were collected (Figure S1 available online) and compared with the spectra of monomeric Ub. Differences in the signal positions,

Table 1. Alignment Tensor Characteristics for K11-Ub_2

Ub	S_{xx}[a]	S_{yy}[a]	S_{zz}[a]	α[b]	β[b]	γ[b]	r[c]	Q[d]
Distal	14.16 (0.48)	16.51 (0.67)	−30.67 (0.80)	285 (1)	40 (1)	296 (11)	0.99	0.05
Proximal	1.44 (0.54)	20.41 (0.58)	−21.85 (0.56)	211 (1)	131 (1)	149 (2)	0.99	0.10
Distal 150 mM NaCl	11.53 (0.45)	17.35 (0.64)	−28.88 (0.71)	294 (1)	38 (1)	292 (5)	0.99	0.05
Proximal 150 mM NaCl	−1.03 (0.56)	−22.95 (0.64)	23.98 (0.62)	135 (1)	63 (1)	303 (2)	0.99	0.11
Proximal 150 mM NaCl[e]	−1.03 (0.56)	23.98 (0.62)	−22.95 (0.64)	191 (1)	138 (1)	138 (2)	0.99	0.11

[a]The principal values of the alignment tensor (in Hz) were ordered as $|S_{zz}| \geq |S_{yy}| \geq |S_{xx}|$. Errors (in parentheses) are estimated using 10,000 Monte Carlo trials.
[b]Euler angles (in degrees) according to the y-convention characterize the principal axes frame of the alignment tensor with respect to the PDB coordinate frame of 1D3Z.
[c]Pearson's correlation coefficient.
[d]Quality factor for RDCs (Clore and Garrett, 1999). Lower Q means better agreement.
[e]The tensor characteristics after switching S_{yy} and S_{zz}.

nonenzymatic chain assembly (Castañeda et al., 2011). The CSP patterns observed in the all-natural K11-Ub_2 are very similar to those shown in Figure 1, suggesting that the introduced chain-terminating mutations had no effect on the structural properties of K11-Ub_2. We also compared spectra of the middle Ub in K11-Ub_3, with the spectra of the proximal Ub and distal Ub in K11-Ub_2. The resulting CSP patterns (Figures 1H and 1I) are strikingly similar to those of the distal Ub and proximal Ub, respectively, in K11-Ub_2 (Figure 1A). This is not unexpected, because the middle Ub in Ub_3 is distal to the proximal Ub and at the same time proximal to the distal Ub. These results indicate that no additional Ub/Ub interactions are present in K11-Ub_3 compared to K11-Ub_2. Therefore, we conclude that K11-Ub_2 can be used as the smallest structural model for understanding structural properties of longer K11-linked chains.

Structural Characterization of K11-Ub_2 in Solution

RDC Measurements

Residual dipolar couplings (RDCs) are a powerful source of information on intermolecular orientation and positioning in protein-protein complexes (Berlin et al., 2010). The RDC of a ^{15}N-^{1}H pair is sensitive to the orientation of the N-H vector with respect to the alignment tensor of the molecule. We collected RDCs of each Ub separately in K11-Ub_2 using 5% C12E5/hexanol as an alignment medium. For each Ub, the alignment tensor was determined from the RDCs using atom coordinates from monoUb solution structure (PDB ID 1D3Z) or from the individual Ub units in each crystal structure of K11-Ub_2 (Table 1; Table S1). The best agreement (Pearson's $r \geq 0.99$) between experimental and back-calculated RDC values for each individual Ub was obtained with 1D3Z (Figures 1F and 1G). Note that the excellent agreement obtained here for the proximal Ub further suggests that the large CSPs observed in the proximal Ub (Figure 1B) are due to isopeptide bond formation and not to changes in the structure of this Ub.

Assuming that the two Ubs in K11-Ub_2 orient together as a single entity, hence with a common alignment tensor, their relative orientation can be obtained by a rigid-body rotation that brings the principal axes of their alignment tensors parallel to each other (Fushman et al., 2004). Out of the eight possible arrangements of the two Ubs due to degenerate orientations and positioning (Fushman et al., 2004), only two are consistent with the isopeptide linkage between the C terminus of the distal Ub and K11 of the proximal Ub (Figures 2A and 2B). The RDCs back-calculated from these structures are in good agreement ($r = 0.96$, $Q = 0.2$), with the experimental RDCs for both distal and proximal Ub analyzed together (Figure 3; Table 2).

Site-Directed Spin Labeling

We then used site-directed spin labeling to independently verify the RDC-derived structures of K11-Ub_2. We attached a paramagnetic spin label (MTSL) to residue 36 in the distal Ub and collected interdomain distance information from paramagnetic relaxation enhancement (PRE) effects induced in the proximal Ub.

The PRE attenuation profile of spin-labeled I36C monoUb (used here both as control and as a mimic of MTSL on the distal Ub) is shown in Figure 2C. In the presence of the paramagnetic spin label, signals for residues 8–13, 34–42, and 69–72 were completely attenuated. By converting the attenuations into distance constraints, the position of the MTSL's unpaired electron was found to be near residue 36, as expected (Figure 2). The back-calculated PRE attenuation profile is in excellent agreement with experiment. When MTSL was attached to I36C of the distal Ub in K11-Ub_2, a significant number of attenuations ($I/I_0 < 0.5$) were observed for signals in the proximal Ub (Figure 2D), particularly for residues 7–14, 33–41, and 69–76. The PRE attenuations and the back-calculated MTSL's positions for both Ubs were mapped onto the two putative RDC-derived structures (Figure 2). The results indicate that of the two structures, only the one in Figure 2B complies with the distance constraints imposed by the PREs. The relative positioning of the two Ubs was optimized by translating one Ub along the z axis of the alignment tensor such that the spin label positions overlapped. Using this structure and the PREs for both the distal and proximal Ub taken together, the back-calculated PRE attenuation profile for K11-Ub_2 (Figure 2E) is in excellent agreement with the experimental data.

^{15}N Relaxation Measurements

Another physical characteristic sensitive to the shape of a molecule and interdomain orientation is molecular tumbling (rotational diffusion), accessible through NMR relaxation measurements (Fushman et al., 2004). ^{15}N relaxation rates R_1 and R_2 and {^{1}H}-^{15}N steady-state hetNOEs for each Ub in K11-Ub_2 are shown in Figure S2. The average ^{15}N T_1 relaxation time is 727 ms ± 34 ms and 754 ms ± 33 ms for the distal Ub and the proximal Ub, respectively. These values, together with ^{1}H T_2

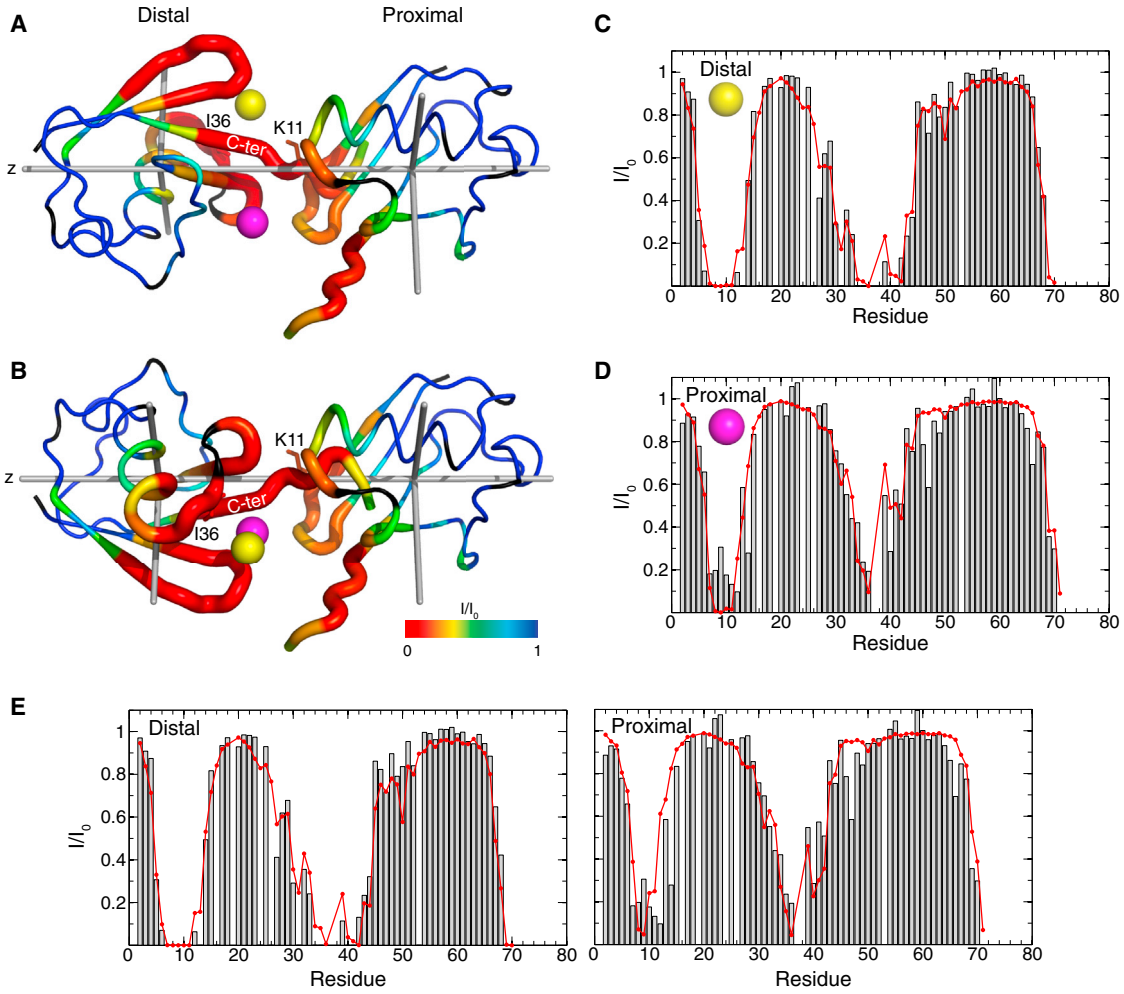

Figure 2. Structure Verification Using Site-Directed Spin Labeling

(A and B) Putative K11-Ub_2 structures derived from RDC data. The structures differ by a 180° rotation of the distal Ub about the z axis of the alignment tensor. Alignment tensor axes are shown as rods; the z axis is horizontal. PRE effects from MTSL attached to I36C of the distal Ub are mapped onto the structures via backbone thickness and color coding (see legend). Spheres indicate the back-calculated positions of the MTSL's unpaired electron derived from the PREs in I36C-MTSL-labeled Ub as a mimic of the distal Ub (yellow) and from the PREs in the proximal Ub (magenta).

(C–E) Experimental (gray bars) and back-calculated (red line) attenuation profiles for the I36C-MTSL Ub (C), the proximal Ub (D), and for the distal and proximal Ubs taken together (E) using the structure in (B).

data, are consistent with tumbling of a molecular species of 17 kDa to 20 kDa, as expected for Ub_2 (Varadan et al., 2002, 2004, 2005). These data suggest that the Ubs in K11-Ub_2 tumble together as a single entity in solution rather than as independent beads on a flexible string. Near-zero or negative hetNOE values, indicative of unrestricted backbone motions, are observed only for the free C terminus of the proximal Ub. By contrast, the hetNOEs for the C terminus of the distal Ub are > 0.4, indicative of the constraints imposed by its tethering to K11 of the proximal Ub. Accordingly, the backbone order parameters (S^2) are very similar across both Ubs (and comparable to monoUb [Fushman et al., 2004]), with the overall high S^2 values indicative of a well-defined structure and lower S^2 values reflecting increased flexibility only for residues 8–12 (β1/β2 loop) and the C termini of both Ubs. A similar behavior was previously observed in K48-Ub_2 (Fushman et al., 2004).

The ratio ρ of backbone ^{15}N relaxation rates (Equation 2) is sensitive to the orientation of the amide N-H vector with respect to the principal axes frame of the rotational diffusion tensor (Fushman et al., 2004). The rotational diffusion tensor was determined for each Ub separately using ROTDIF (Walker et al., 2004) (Table 3; Figure S2). The principal components of the rotational diffusion tensors and the overall rotational correlation times for both Ubs were similar (Table 3), further indicating that to a first approximation, they tumble together as a single entity twice the size of a Ub monomer. Therefore, we obtained the relative orientation of the Ubs in K11-Ub_2 by aligning their diffusion tensors in a similar manner as for the alignment tensors (see above). The resulting structure of K11-Ub_2 is shown in Figure 4B.

The ^{15}N relaxation-derived structure is very similar to the structure derived from RDC measurements (Figure 4). This is an important observation as relaxation and RDC measurements probe

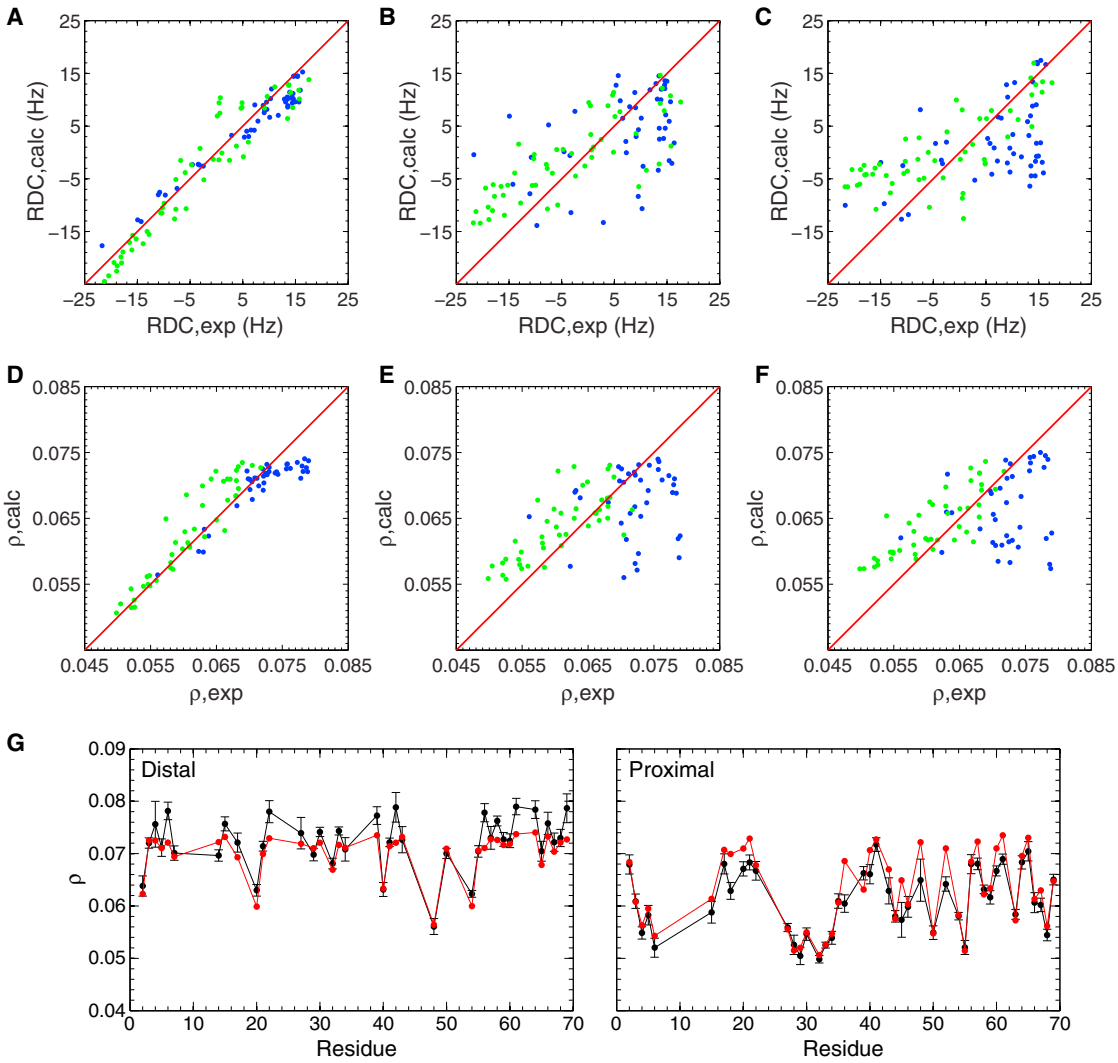

Figure 3. Comparing K11-Ub$_2$ Structures with RDC and ^{15}N Relaxation Data

(A–F) Comparison between experimental and back-calculated (A–C) RDCs or (D–G) ^{15}N relaxation ρ values for both distal Ub (blue) and proximal Ub (green), taken together, analyzed using the RDC-derived solution structure of K11-Ub$_2$ (A), the ^{15}N relaxation-derived solution structure of K11-Ub$_2$ (D), the crystal structure from PDB ID 2XEW (B and E), and the crystal structure from PDB ID 3NOB (C and F).

(G) Experimental (black) and back-calculated (red) ρ values (Equation 2) determined using the relaxation-derived structure (Figure 4B) for both distal and proximal Ubs taken together.

See also Figure S2.

very different physical phenomena: namely, molecular tumbling and orientational sampling. Furthermore, ^{15}N relaxation rates monitor dynamics on a timescale up to tens of nanoseconds while RDCs reflect motions occurring over a much wider time range, up to milliseconds or longer. Note that the domain-alignment methods used here provide a time-averaged conformation of Ub$_2$, which depends on the time scale and the extent of interdomain motions in the chain (Fushman et al., 2004). Because of the differences in the time windows between the relaxation and RDC measurements, the time-averaged interdomain orientation derived from these data could be different. The very fact that these two different measurements result in similar interdomain orientations lends credence to these structures. It should be emphasized here that the back-calculated ρ values using the RDC-derived structure are in good agreement with the experimental ρ data and, vice versa, the RDCs back-calculated using the ^{15}N relaxation-derived structure are in very good agreement with the experimental RDC data (Table 2).

The Effect of Salt on the Structure of K11-Ub$_2$

To assess the effect of physiological salt concentration on the conformation of K11-Ub$_2$ and to test the possibility that electrostatics may contribute to Ub/Ub interactions in K11-Ub$_2$, we measured CSPs and RDCs in the presence of 150 mmol/L (mM) NaCl at pH 6.8 (Figures S3 and S4; Table 1). Overall, the CSP pattern remained the same as in the absence of NaCl. However, small but notable increases in the CSPs were observed for residues 5–15, 31–34, and 70–71 in the distal Ub (Figure S4C). In the proximal Ub, increased CSPs were observed for residues 7, 8, 12, and 13 and in the C terminus.

Table 2. Agreement of Experimental with Back-Calculated ^{15}N Relaxation ρ and RDC Values for Both Ub Units Taken Together in Various K11-Ub_2 Structures

Ub_2 Structure[a]	Data Type[b]	r[c]	Q[d]
Relaxation	ρ	0.919	0.281
RDC	ρ	0.916	0.285
2XEW	ρ	0.555	0.597
3NOB	ρ	0.520	0.620
1D3Z mimic of 2XEW	ρ	0.610	0.565
1D3Z mimic of 3NOB	ρ	0.586	0.583
Relaxation	RDC	0.946	0.233
RDC	RDC	0.963	0.200
2XEW	RDC	0.678	0.516
3NOB	RDC	0.611	0.556
1D3Z mimic of 2XEW	RDC	0.691	0.507
1D3Z mimic of 3NOB	RDC	0.646	0.536
RDC	RDC 150 mM NaCl	0.956	0.214
RDC, 150 mM NaCl	RDC 150 mM NaCl	0.964	0.188
2XEW	RDC 150 mM NaCl	0.772	0.443
3NOB	RDC 150 mM NaCl	0.746	0.464
1D3Z mimic of 2XEW	RDC 150 mM NaCl	0.789	0.428
1D3Z mimic of 3NOB	RDC 150 mM NaCl	0.772	0.444

[a]Relaxation- and RDC-derived structures were determined using NMR data in the absence of salt, unless otherwise noted.
[b]ρ is defined in Equation 2.
[c]Pearson's correlation coefficient.
[d]Quality factor as defined for ^{15}N relaxation ρ values (Ghose et al., 2001) and RDCs (Clore and Garrett, 1999).

The RDC data for K11-Ub_2 in 150 mM NaCl are quite similar to the data collected in the absence of salt (Figure S3). The alignment tensors of the distal Ub are very similar across the two data sets, regardless of the salt concentration (Table 1). The proximal Ub, however, appeared to have different alignment tensor characteristics, particularly the orientation of the tensor's axes. Because the RDCs for the proximal Ub in 150 mM NaCl correlate well with the RDCs in the absence of salt (Figure S3) and because of the strong rhombicity of its alignment tensor ($S_{xx} \approx 0$; $|S_{yy}| \approx |S_{zz}|$), we examined the possibility that the assignment of the S_{yy} and S_{zz} axes could have been switched as a result of the absolute values of the corresponding principal components being similar (Figure S4E). Indeed, the corrected alignment tensor matches well the one at no salt, and the back-calculated RDCs from the structure determined with revised Euler angles are in excellent agreement with experiment (Figure S4F; Table 3). The RDC-derived structure of K11-Ub_2 in 150 mM NaCl is shown in Figure 4C.

A comparison of the K11-Ub_2 solution structures in the absence and presence of NaCl shows that the distal Ub has very similar orientations with respect to the alignment tensor of the molecule. By contrast, the proximal Ub in 150 mM NaCl exhibited a twist by 16–21° relative to the proximal Ub in the absence of salt (see also Table 1). This change in orientation of the proximal Ub has brought L8 of both Ubs closer to each other and also brought the C terminus of the proximal Ub closer to the distal Ub (Figures 4C and 5A–5C). This is fully consistent with the observed increase in CSPs for these residues in 150 mM NaCl (Figure S4).

Small-Angle Neutron Scattering Studies of K11-Ub_2

To independently verify the effect of salt on the conformation of K11-Ub_2 we performed SANS studies of this chain at different NaCl concentrations in solution (Figure 5G and 5H). From Guinier plot analysis, the radius of gyration (R_g) decreased from 19.2 Å to 18.5 Å upon addition of 150 mM NaCl, and decreased even further to 17.7 Å at 500 mM NaCl (Table S2). These values are within range of expected R_g values computed from our RDC-derived structures. Furthermore, at intermediate values of q ($0.2\ Å^{-1} > q > 0.05\ Å^{-1}$), $I(q)$ increased as a function of salt (Figure 5G). The changes in $I(q)$ reflect a change of the atom-atom pairwise distance distribution, $P(r)$. Indeed, the $P(r)$ profiles in Figure 5H indicate that the number of pairwise Ub-Ub distances >30 Å decreases as salt concentration is increased. [No change is observed in the $P(r)$ plot for $r < 30$ Å; this confirms that the structures of the Ub units are unchanged in the presence of salt.] In other words, the SANS data indicate that increasing salt concentration brings the two Ubs closer together. Remarkably, the $P(r)$ profiles calculated from our RDC-derived structures at 0 and 150 mM NaCl do capture the relative changes in the experimental $P(r)$ profiles as a function of salt (Figure 5J). Thus, the SANS data lend credence to our RDC-derived structures and corroborate the above conclusions (stemming from CSPs and RDCs) that increasing salt concentration compacts the structure of K11-Ub_2.

Comparison with Crystal Structures of K11-Ub_2

The solution structures of K11-Ub_2 are compared to the two crystal structures of K11-Ub_2 in Figure 5. It is apparent that the Ub/Ub orientations vary widely across the four structures. Previous analyses of the crystal structures suggested a number of putative Ub/Ub interactions, particularly involving residues 24, 39, 52, 72, and 74 of the distal Ub (Bremm et al., 2010) or residues 7–13, 34–42, and 69–76 of both the distal and proximal Ubs (Matsumoto et al., 2010). However, none of these residues exhibit significant CSPs in the absence of salt, with the exception of residues 72–76 (linker region) of the distal Ub.

Neither of the two crystal structures of K11-Ub_2 is consistent with our solution NMR data (Figure 3). Little or no correlation exists between experimental data (RDC, ^{15}N relaxation, PREs) and the corresponding back-calculated values for these crystal structures (Table 3). To eliminate the possibility that the poor agreement with the crystal structures of Ub_2 reflects the differences between the crystal and solution structures of the individual Ub units (Table S1) rather than of the Ub_2 structures, we reconstructed the Ub/Ub orientations of both crystal structures using the solution structure (1D3Z) for each Ub unit; these structures will be referred to as 1D3Z mimics of the crystal structures. This, however, did not improve the agreement with experimental ^{15}N relaxation ρ or RDC data (Table 3). Furthermore, the $P(r)$ profiles and R_g values computed from the crystal structures are markedly different from the experimentally observed $P(r)$ and R_g values (Figure 5H and 5I).

Increasing salt concentration to 150 mM NaCl altered the relative orientation and positioning of the two Ubs in K11-Ub_2, as evident from the CSP, RDC, and SANS data. As a result, the

Table 3. Diffusion Tensor Characteristics for K11-Ub_2

Ub	D_{xx}[a]	D_{yy}[a]	D_{zz}[a]	α[b]	β[b]	γ[b]	τ_c[c] (ns)	Anisotropy[d]	Rhombicity[d]	Probability[e]
Distal	1.69 (0.09)	1.81 (0.07)	2.53 (0.13)	109 (8)	145 (5)	152 (19)	8.29 (0.24)	1.44 (0.09)	0.21 (0.03)	2.71×10^{-13} (f/iso) 6.77×10^{-3} (f/ax)
Proximal	1.64 (0.05)	1.82 (0.05)	2.35 (0.09)	38 (4)	44 (5)	105 (16)	8.61 (0.17)	1.36 (0.06)	0.43 (0.04)	7.55×10^{-23} (f/iso) 3.02×10^{-4} (f/ax)

[a]Principal values of the diffusion tensor, in 10^7 s^{-1}. Errors (in parentheses) were estimated using 1000 Monte Carlo trials.
[b]Euler angles (in degrees) according to the y-convention characterize the principal axes frame of the diffusion tensor with respect to the PDB coordinate frame of 1D3Z.
[c]Overall rotational correlation time.
[d]Calculated as defined (Fushman et al., 2004).
[e]F-test-derived probability that the improvement in the fit for a fully anisotropic (f) diffusion tensor over either axially symmetric (ax) or isotropic (iso) diffusion tensor models could have occurred by chance.

average conformation of K11-Ub_2 moved toward the crystal structure 3NOB (Figures 5B, 5E, and 5K). At this salt concentration, correlations between experimental and back-calculated RDC values improved slightly for either crystal structure (Figure S5; Table 3), but the highest correlation coefficient is still significantly lower (and a significantly higher Q) than for either RDC-derived structure.

From Figure 5K, it is tempting to imagine that the RDC-derived solution structures (or the ^{15}N relaxation-derived structure) of K11-Ub_2 could be a result of motional averaging of the two crystal structures. To examine this possibility, we predicted the RDCs resulting from a population-weighted dynamic equilibrium of the crystal structures (see Figure S6; Table S3). Our results showed that a combination of the two crystal structures cannot reproduce the experimental RDC values either in the absence or presence of salt ($r < 0.5$). By contrast, the RDCs predicted based on the NMR-derived structures of K11-Ub_2 are in good agreement ($r = 0.95$, Q = 0.23) with the experimental data.

A close inspection shows, however, that even for the NMR-derived structures of K11-Ub_2, the agreement between back-calculated and experimental RDCs is not perfect as the Q values are noticeably higher than for the individual Ub units (compare Table S1 and Table 3). This suggests that the NMR-derived structures alone, although capturing the time-averaged structural features of K11-Ub_2 in solution, might not fully represent the conformational ensemble of the chain. We therefore considered the possibility that the conformational ensemble of K11-Ub_2 comprises both the RDC-derived and the crystal structures of the chain. For this we predicted RDC values averaged over an ensemble of 2, 3, or 4 conformers (considering all possible combinations of the four available structures of K11-Ub_2) and adjusted their populations in order to obtain the best agreement with the experimental RDCs (see Supplemental Information, equation S1). Only a marginal improvement in the agreement was obtained for the experimental data at 0 mM NaCl ($r = 0.96$, Q = 0.21; Table S3). For RDC data in the presence of salt, a combination of three structures (the RDC-derived structures at 0 mM and 150 mM NaCl and PDB ID 3NOB, with the weights of 61%, 14%, and 25%, respectively) modestly improved the agreement with experiment ($r = 0.97$, Q = 0.18). Interestingly, a similar improvement was obtained for a combination of the RDC-derived structure at 0 mM and the crystal structure 3NOB (populated at 70% and 30%, respectively; Table S3). These results imply that the RDC-derived structure at 150 mM NaCl may reflect a dynamic equilibrium between the RDC-derived structure in the absence of NaCl (representing the predominantly populated conformer) and some lesser-populated conformers that are structurally more compact and possibly close to the 3NOB structure. This suggests that the observed compaction at increased salt concentration might reflect a change in the relative populations within the conformational ensemble rather than merely a change in the single conformation of K11-Ub_2. Overall, we conclude that consideration of the crystal structures as possible conformers of K11-Ub_2 contributed only minimally to improving the agreement with solution NMR data. Other conformers, currently unknown, might be necessary to perfect the agreement with experiment.

Ligand-Binding Properties of K11-Ub_2

Prior studies of K48-Ub_2 and K63-Ub_2 have provided significant structural and functional evidence that polyUb chains of different linkages bind to Ub-binding domains differently (Raasi et al., 2005; Sims and Cohen, 2009; Varadan et al., 2004, 2005). To examine how the structural and dynamical features of K11-Ub_2 impact the chain's ability to recognize target proteins, we conducted NMR titration studies of K11-Ub_2 with known Ub-receptors associated with degradative and nonproteolytic pathways: (1) Ub-associated domain (UBA) of Ubiquilin-1 (also known as hPLIC-1, human homolog of the yeast proteasomal shuttle protein Dsk2), which binds monoUb with μM affinity and shows no chain-linkage selectivity (Zhang et al., 2008); (2) UBA2 domain of the proteasomal shuttle protein hHR23a, which preferentially recognizes K48-linked Ub chains (Raasi et al., 2005; Varadan et al., 2005); and (3) a tandem Ub-interacting motif (tUIM) from Rap80, a protein involved in nonproteolytic pathways that preferentially binds K63-linked Ub chains (Sims and Cohen, 2009). We titrated an unlabeled ligand into a sample of K11-Ub_2 ^{15}N-enriched on either the distal or the proximal Ub, and backbone amide signals were monitored as a function of ligand concentration using standard ^1H-^{15}N NMR experiments. Binding affinities were determined from fitting residue-specific titration curves as described in Experimental Procedures.

Binding to Ubiquilin-1 UBA

Figures 6A and 6B show CSPs of residues in K11-Ub_2 at saturating concentrations of Ubiquilin-1 UBA (UQ1-UBA). These CSPs map the UBA-interacting surface on Ub to those residues centered around the hydrophobic patch (residues L8, I44, and V70). Note that the overall CSP pattern and magnitudes, as

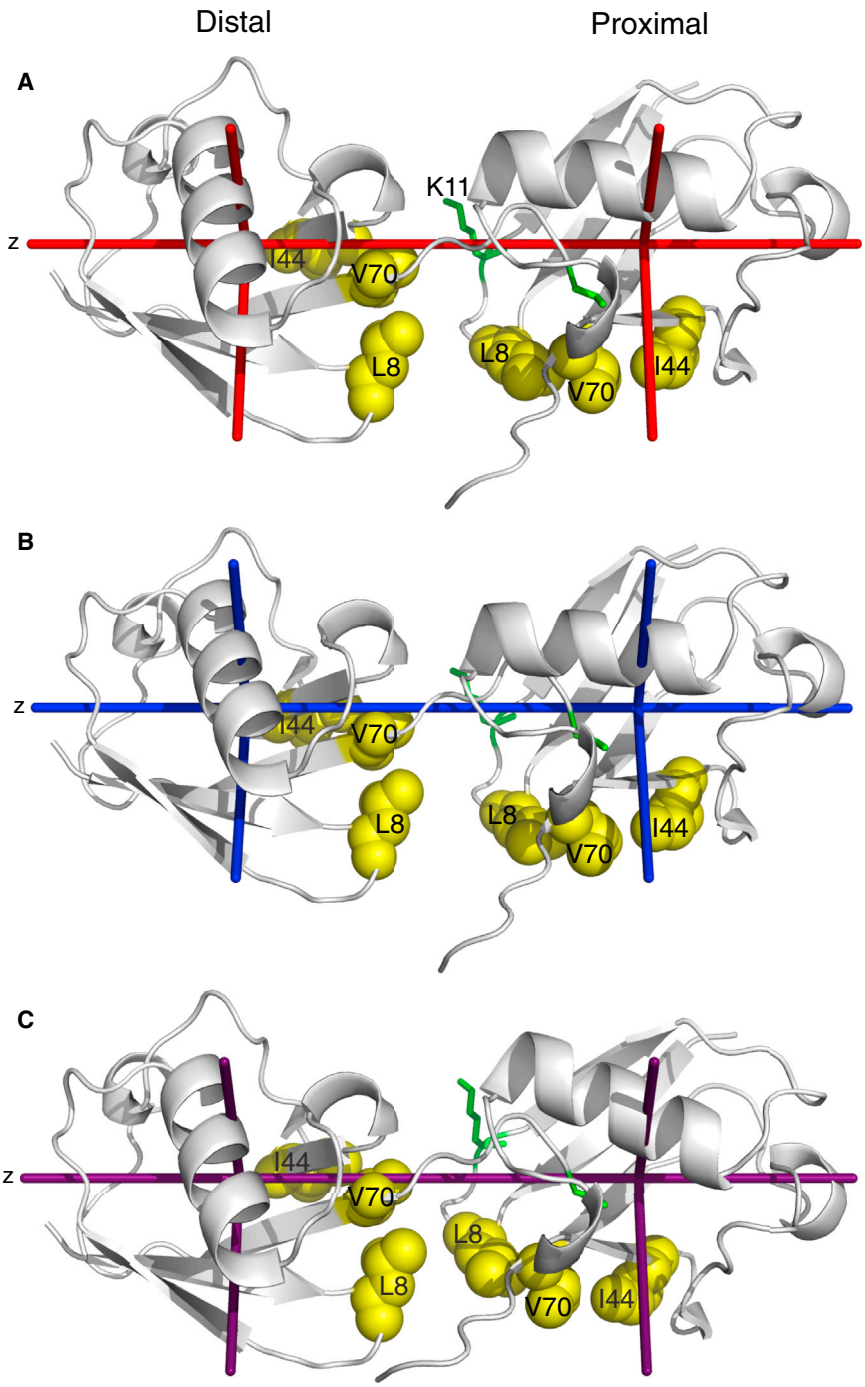

Figure 4. Solution Structures of K11-Ub_2 at pH 6.8

Structures derived from RDC data in the absence (A) and presence (C) of NaCl. Structure derived from ^{15}N relaxation data (B) in the absence of NaCl. The structure in (A) is the same as in Figure 2B. Axes of the alignment and diffusion tensors are shown as colored rods, with the z axis of the tensor oriented horizontally. For all structures, the distance between the centers of mass of the two Ubs was set to 28 Å, as determined from the PRE data (Figure 2).

See also Figures S3 and S4.

well as NMR signal shift trajectories are very similar across both Ubs (Figures S8 and S9). Moreover, the CSP patterns of K11-Ub_2 match the CSP patterns of monoUb, K48-Ub_2, and K63-Ub_2 at saturation with UQ1-UBA (Zhang et al., 2008).

Inspection of the titration curves for the proximal Ub revealed a sigmoidal shape, which prompted us to use a two-independent-binding-sites model (Varadan et al., 2005) for UQ1-UBA binding to K11-Ub_2 (Figure S8). The average K_d was 2.9 μM and 10 μM for the distal Ub and proximal Ub, respectively (Table 4), well within the K_d values (4–32 μM) reported for monoUb, K48-Ub_2, and K63-Ub_2 (Zhang et al., 2008). To verify the 2:1 stoichiometry of the UQ1-UBA complex with K11-Ub_2, ^{15}N T_1 relaxation measurements were performed at saturation (ligand:protein molar ratio of 6:1). The ^{15}N T_1 was 1101 ms ± 71 ms and 1167 ms ± 109 ms for the distal and proximal Ub, respectively (Figure S7). These numbers correspond to tumbling of a molecular species of 30–33 kDa, consistent with two UBA molecules bound to K11-Ub_2 (the expected molecular weight is 28 kDa). Therefore, we conclude that UQ1-UBA has similar affinity for monoUb and either Ub in K11-, K48-, or K63-linked Ub_2 and is not linkage selective (Raasi et al., 2005; Zhang et al., 2008).

Binding to hHR23a UBA2

The UBA2 domain of hHR23a binds preferentially to K48-linked chains (Raasi et al., 2005) and in a sandwich-like mode involving contacts with the hydrophobic patches of both Ub units and the linker region (Varadan et al., 2005). UBA2 also binds specifically but weakly to both monoUb (Mueller et al., 2004; Ryu et al., 2003) and K63-Ub_2 (Varadan et al., 2004). Our NMR data show that UBA2 interacts specifically with the hydrophobic-patch surfaces of both Ubs in K11-Ub_2. The overall CSP pattern at titration endpoint (Figures 6C and 6D) is generally similar across both Ub units, with the distal Ub exhibiting slightly larger CSPs. Interestingly, the CSP pattern of the distal Ub is nearly identical to that of either monoUb or the distal Ub of K63-Ub_2 upon saturation with UBA2 (Varadan et al., 2004).

The affinity of K11-Ub_2 for UBA2 was determined assuming that only one UBA2 molecule is bound to either Ub of K11-Ub_2, but not to both Ubs simultaneously. (The 2:1 stoichiometry model, i.e., two UBA2 molecules binding K11-Ub_2, substantially increased the residuals of fit.) The K_d values obtained for the distal and proximal Ubs in K11-Ub_2 were 155 μM and 197 μM, respectively (Table 4), indicating that the UBA2 binding to each

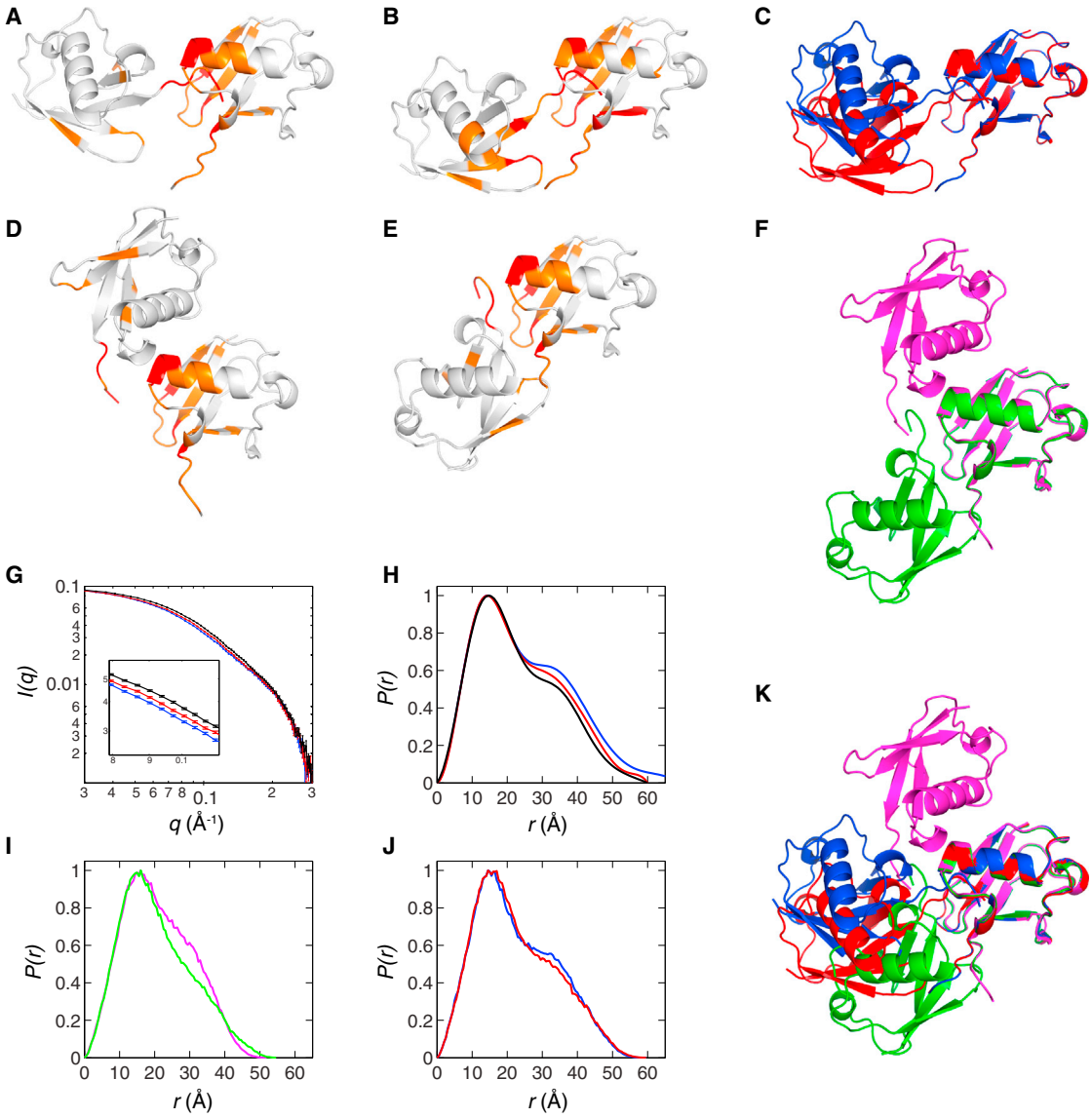

Figure 5. Comparison of the Solution and Crystal Structures of K11-Ub_2

(A–C) RDC-derived solution structures from this work at 0 mM NaCl (A) and 150 mM NaCl (B) and superimposed by the proximal Ub (C).

(D–F) Crystal structures from PDB IDs 2XEW (D) and 3NOB (E), and superimposed by the proximal Ub (F).

CSPs in the absence of salt are mapped onto all structures shown in (A), (D), and (E) except for the structure in (B), where CSPs at 150 mM NaCl were used. Residues with CSPs > 0.10 ppm are colored red and with 0.03 < CSPs < 0.10 ppm are colored orange.

(G and H) Experimental SANS *I*(*q*) and *P*(*r*) plots for K11-Ub_2 at 0 mM NaCl (blue), 150 mM NaCl (red), and 500 mM NaCl (black). *I*(*q*) curves were scaled such that protein concentrations were equal for all three salt conditions. Error bars on the SANS data represent the combined standard uncertainty of the data collection.

(I and J) Calculated *P*(*r*) plots from (I) the X-ray structures 2XEW (magenta) and 3NOB (green), and (J) the RDC-derived structures at 0 mM NaCl (blue) and 150 mM NaCl (red).

(K) All structures, from panels (A), (B), (D), and (E), superimposed by the proximal Ub and colored blue, red, magenta, and green, respectively.

The same coloring scheme is used in panels (C) and (F). All structures in this figure are oriented such that the proximal Ub (on the right) is in the same orientation. See also Figure S6.

Ub in K11-Ub_2 is significantly weaker than to K48-Ub_2 ($K_d \approx 18$ μM) (Varadan et al., 2005) yet somewhat stronger than to K63-Ub_2 (Varadan et al., 2004) ($K_d > 200$ μM) or monoUb ($K_d \approx 400$ μM) (Mueller et al., 2004; Ryu et al., 2003). These results are in line with a recent MS study (Sokratous et al., 2012) and suggest that UBA2 is selective for K48-linked chains over K11- and K63-linked chains.

We used ^{15}N T_1 measurements to examine the stoichiometry of binding at the titration endpoint ([UBA2]/[Ub_2] ~6). We obtained 959 ms ± 44 ms and 1006 ms ± 41 ms for the distal and proximal Ubs, respectively, which are significantly lower than the ^{15}N T_1 values (1095 ms and 1118 ms) reported for K48-Ub_2 with two UBA2 molecules bound (Varadan et al., 2005) as well as the ^{15}N T_1 values for K11-Ub_2 in complex with

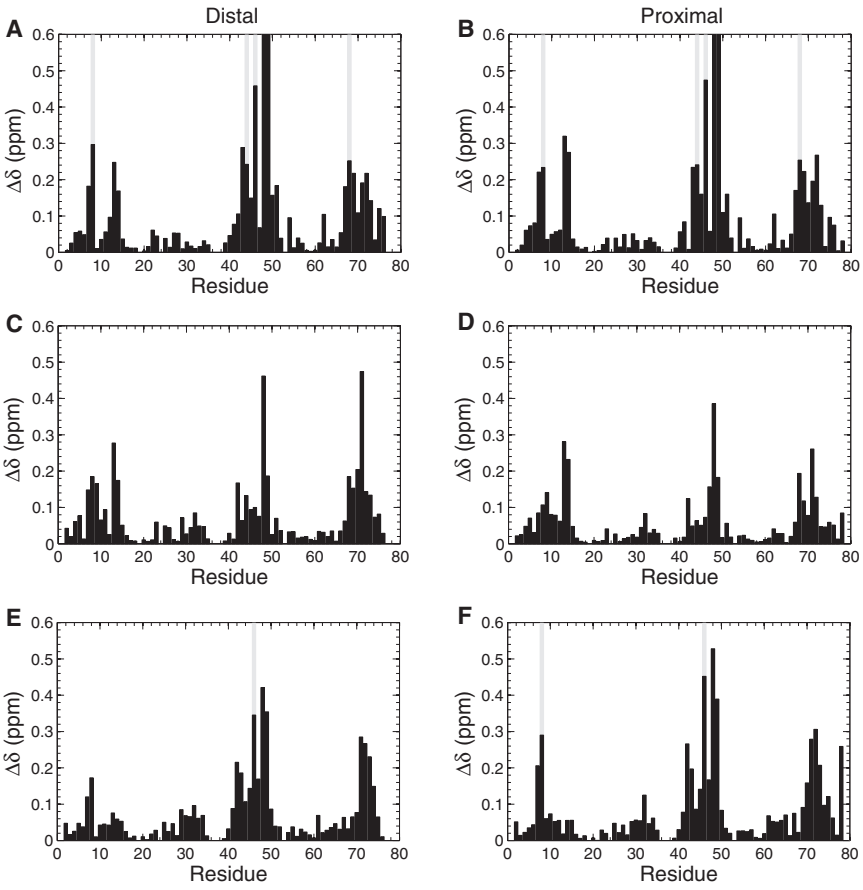

Figure 6. Mapping Ligand Binding to K11-Ub_2

Shown are CSPs in K11-Ub_2 at titration endpoint with (A and B) Ubiquilin-1 UBA, (C and D) hHR23a UBA2, and (E and F) Rap80 tUIM. "Residue 78" in the proximal Ub represents the K11 isopeptide linkage signal. Residues whose signals broadened significantly or attenuated during the titration are marked with gray bars.

See also Figures S7–S10 and S12.

two UQ1-UBA molecules (see above). The ^{15}N T_1 values for the UBA2:K11-Ub_2 complex suggest a molecular complex intermediate between a 1:1 (23 kDa) and a 2:1 (29 kDa) UBA2:Ub_2 complex. Interestingly, several residues (8, 11, 12, 45, 70, 72, 73, and the K11 isopeptide) in the proximal Ub exhibited a change in signal trajectories above [UBA2]/[Ub_2]~2 (Figure S9D). The new directions for these signal trajectories match the trajectories of the same residues in the distal Ub. We speculate that these observations reflect binding of a second Ub occurring at the endpoint of titration and resulting in somewhat higher than expected ^{15}N T_1 values. Indeed, if we propagate the average ^{15}N T_1 values to saturation, the results (998 ms and 1056 ms) are closer to those observed for K48-Ub_2 with two UBA2 molecules bound.

Binding to Rap80 tUIM

The Rap80 protein interacts preferentially with K63-linked polyUb chains via avid and specific interactions of its two UIMs (Sato et al., 2009; Sims and Cohen, 2009). A Rap80 construct containing just the tUIM binds to K63-Ub_2 (K_d = 22 μM) tighter than to K48-Ub_2 (K_d = 157 μM) (Sims and Cohen, 2009). The tUIM forms a 1:1 stoichiometric complex with K63-Ub_2 in which each UIM interacts with a specific Ub unit (Sato et al., 2009), whereas such a binding mode does not occur with K48-Ub_2 (Sims and Cohen, 2009). We therefore decided to examine whether K11-Ub_2 is capable of avid binding to tUIM.

To set the stage for examining Rap80 tUIM binding to K11-Ub_2, we mapped the tUIM-interacting surfaces on K63-Ub_2 and K48-Ub_2 (Figure S10). The CSP patterns for K63-Ub_2 upon tUIM binding were very distinct across the two Ub units, specifically for residues 4–16 and 62–76. By contrast, the CSP patterns for K48-Ub_2 were almost identical across both Ubs. The CSPs in K11-Ub_2 at the titration endpoint (Figure 6) were quite similar across the distal and proximal Ubs, suggesting that tUIM interacts with K11-Ub_2 via a binding mode similar to K48-Ub_2. Note, however, that we observed small but specific CSPs for residues 61–68 of the proximal Ub; the same residues exhibit strong CSPs in the proximal Ub of K63-Ub_2.

The tUIM affinity for the proximal Ub of K11-Ub_2 (K_d = 68 μM) is 2-fold stronger than for the distal Ub (K_d = 134 μM) (Table 4). Just as with the UBA2 titration data, the binding affinities were determined assuming that a single tUIM molecule is bound to K11-Ub_2 at a time (Figure S8). The choice of the binding model is also supported by the ^{15}N T_1 values at the titration endpoint (Table 4): 972 ms ± 60 ms and 1078 ms ± 68 ms, for the distal and proximal Ubs, respectively (Figure S7). These numbers correspond to an apparent molecular weight between 28 kDa and 32 kDa, which is intermediate between a 1:1 (25 kDa) and a 2:1 tUIM:Ub_2 complex (33 kDa). Together with CSPs, these data suggest that Rap80 does not interact with K11-Ub_2 in an avid-binding mode as with K63-Ub_2.

DISCUSSION

We determined three-dimensional structures of K11-Ub_2 in solution at neutral pH in the absence and presence of salt. These structures are consistent with a range of experimental data, including CSPs, RDCs, PREs, ^{15}N relaxation rates, and SANS, but differ dramatically from the published crystal structures of K11-Ub_2. Moreover, the strong similarity between the CSPs in K11-Ub_3 and Ub_2 indicates that the Ub/Ub contacts and structural features of K11-Ub_2 are preserved in longer chains.

The inter-Ub orientations and contacts observed here are unique to the K11 linkage. The small but systematic CSPs observed for residues at or near the L8-I44-V70 hydrophobic surface patch on the distal Ub indicate an interaction between the two Ub units in K11-Ub_2. These contacts differ markedly when compared to K63-Ub_2, in which no detectable noncovalent

Table 4. Summary of Ligand Binding Studies of K11-Ub_2

Protein: Ligand[a]	K_d (μM)[b]	Binding Model	Average ^{15}N T_1 (ms) at Titration Endpoint[b]	[L]:[P] at Titration Endpoint
free K11-Ub_2(^{15}N-D)	-	-	727 ± 34	-
free K11-Ub_2(^{15}N-P)	-	-	754 ± 33	-
K11-Ub_2(^{15}N-D): UQ1-UBA	2.9 ± 2.2[c]	2:1, independent sites	1110 ± 71	≈5:1
K11-Ub_2(^{15}N-P): UQ1-UBA	10.0 ± 3.3[c]	2:1, independent sites	1167 ± 109	≈5:1
K11-Ub_2(^{15}N-D): UBA2	155 ± 22	2:1, one site occupied	959 ± 44	≈6:1
K11-Ub_2(^{15}N-P): UBA2	197 ± 30	2:1, one site occupied	1006 ± 41	≈6:1
K11-Ub_2(^{15}N-D): tUIM	134 ± 18	2:1, one site occupied	972 ± 60	≈6:1
K11-Ub_2(^{15}N-P): tUIM	68 ± 15	2:1, one site occupied	1078 ± 68	≈5:1

[a] ^{15}N-D or ^{15}N-P indicate the ^{15}N enriched Ub (distal or proximal, respectively) in K11-Ub_2.
[b] The errors in K_d values and in average T_1 values are standard errors of the mean over multiple residues.
[c] K_d from the two-independent-binding-sites model.

inter-Ub interactions are present (Varadan et al., 2004), and K48-Ub_2, in which both the NMR data and crystal structure show an extended Ub/Ub interface mediated by the hydrophobic patch residues on both Ubs (Varadan et al., 2002). Interestingly, the CSPs in K11-Ub_2 are largely unchanged over a pH range from 4.5 to 7.6 (Figure S11), in contrast with the strong effect of pH on the solution conformation of K48-linked chains (Varadan et al., 2002). However, both NMR and SANS data suggest that increasing salt concentration brings the hydrophobic patches of the two Ubs closer to each other in K11-Ub_2. This salt-dependent compaction was not observed for other Ub dimers (unpublished data).

Our analysis shows that neither crystal structure of K11-Ub_2 taken separately nor conformational averaging of the crystal structures is consistent with the solution NMR data. This suggests that the published crystal structures of K11-Ub_2 are a consequence of crystal packing forces that may have artificially stabilized and therefore biased the K11-Ub_2 conformations observed in PDB IDs 2XEW and 3NOB. In fact, it has been shown that both Ub/Ub contacts (seen in 2XEW and in 3NOB) are present, as inter- or intrachain contacts, in either crystal structure (Bremm and Komander, 2011).

It should be emphasized here that the NMR-derived structures of K11-Ub_2 inevitably reflect some degree of motional averaging present in solution and therefore should be considered as "time-averaged" conformations rather than single-structure snapshots. In fact, a detailed analysis revealed that both the RDC and ^{15}N relaxation data bear hallmarks of interdomain dynamics. Although to a first approximation, the two Ubs in K11-Ub_2 tumble and align together as a single entity (see above), the ^{15}N relaxation data indicate backbone flexibility in the Ub-Ub linker region, which is evident from the low backbone order parameters and hetNOE values (Figure S2). This implies that the conformation of K11-Ub_2 is not rigidly locked. In fact, we note the differences in the principal values of the alignment tensors for the two Ubs in K11-Ub_2 (Table 1): namely, a nearly axially symmetric ($|S_{xx}| \approx |S_{yy}|$) alignment tensor for the distal Ub and a strongly rhombic ($|S_{yy}| \approx |S_{zz}|$, $S_{xx} \approx 0$) tensor reported by the proximal Ub. The different tensor properties could result from either (1) each Ub interacting differently with the alignment medium or (2) the presence of interdomain mobility in Ub_2 (Tolman and Ruan, 2006). The former seems unlikely, given the chemical and structural similarity of both Ub units and no detectable differences between NMR spectra in the absence and presence of the alignment medium. In addition, the increased RDC-quality factors for Ub_2 compared to those for each Ub unit analyzed separately (Table S1; Table 2) suggest that there are other features of K11-Ub_2 that are not fully captured by a single structure. Likewise, an inspection of the back-calculated ^{15}N ρ values showed that while the ρ pattern in each Ub is reproduced well, the difference in the overall ρ levels between the distal and proximal Ubs is not (Figure 3G).

All these observations suggest the presence of interdomain motions in K11-Ub_2 not accounted for in the single-tumbling-entity model. Note in this regard that for K48-Ub_2, the difference in overall ρ levels between the two Ubs could be reproduced only when a population-weighted dynamic equilibrium between at least two conformations was considered (Ryabov and Fushman, 2006). Similarly to K48-Ub_2, the excellent agreement between the structures of K11-Ub_2, derived from the overall tumbling and from molecular alignment, as well as the consistency of the structures with the PRE data, suggest that these structures represent the predominant conformation of the chain. We speculate that a substantial portion of interdomain motions in K11-Ub_2 occur on a timescale faster than the overall tumbling (τ_c ~10 ns) of the chain. These motions are fast enough to average both the apparent diffusion and alignment tensors, thus resulting in similar structures derived from ^{15}N relaxation and RDC data. On the other hand, the RDC-quality factor for the RDC-derived K11-Ub_2 structure is somewhat higher than for the individual Ub units, suggesting a dynamic equilibrium (on a slower timescale) with other, less populated conformations of the chain. This is further supported by the elevated ^{15}N R_2 values in the vicinity of K11 in the proximal Ub (Figure S2), indicating the presence of interdomain motions on the microsecond timescale.

Combining our solution structures with the crystal structures of K11-Ub_2 provides a glimpse into the range of conformations that this chain can adopt under various conditions (Figure 5K). An adequate representation of the conformational ensemble of K11-Ub_2 might require additional conformers, as inferred from the fact that only a marginal improvement in the (already good) agreement with experimental RDC data was achieved when considering the crystal structures together with the

NMR-derived structures as members of the conformational ensemble of K11-Ub_2 (Table S3). We anticipate that the inclusion of other conformers (likely low populated) would perfect the agreement with experiment. Elucidating the conformational ensemble of K11-Ub_2 will be key to understanding receptor recognition and the function of K11-linked chains in many different signaling pathways and to design of K11 linkage-specific ligands.

The interdomain motions and conformational properties of K11-Ub_2 likely contribute to the ability of K11-linked chains to bind to various receptors in the proteolytic and nonproteolytic signaling pathways via different binding modes. Curiously, K48-linked chains perform similar if not identical functions as K11-linked chains during cell cycle regulation in budding yeast where K11-specific Ub-conjugating E2 enzymes (Ube2C and Ube2S) are absent (Wickliffe et al., 2011a). Perhaps then it is not surprising that K11-linked polyUb may adopt certain features of K48-linked polyUb in higher eukaryotic organisms. It remains to be seen whether K11-linked chains bind directly to proteasomal Ub-receptors (e.g., Rpn10, Rpn13) in a K48-like binding mode. Because K11-linked chains are implicated in nonproteolytic pathways such as NF-κB signaling (Dynek et al., 2010), in which K63-linked chains are also found, K11-linked chains could also adopt a K63-like binding mode in which the presentation of the Ub hydrophobic patches is in a more extended conformation. The binding modes for K11-linked chains remain unknown because no structures have yet been determined for their complexes with (unidentified) target receptors. It is evident from the binding studies conducted herein that K11-Ub_2 does bind both K48-selective (UBA2) and K63-selective (Rap80) receptors. However, K11-Ub_2 binding to these receptors differs from either K48-Ub_2 or K63-Ub_2 both in terms of stoichiometry and affinity. To understand the structural basis for these differences, we constructed preliminary models for engagement of each Ub unit with the binding partners studied here (Figure S12). Our models are consistent with the observed 2:1 stoichiometry of binding and help rationalize the observed differences in the affinities. The K11-Ub_2 structures do not allow simultaneous interaction of a single UBA or tUIM molecule with the hydrophobic patches on both Ub units (as well as with the isopeptide linker in the case of UBA2). These interactions are required for the high-affinity linkage-selective binding of hHR23a UBA2 to K48-Ub_2 and of Rap80 tUIM to K63-Ub_2 (Sims and Cohen, 2009; Varadan et al., 2005). By contrast, such a binding mode is not required for UQ1-UBA (Zhang et al., 2008), which shows comparable affinity for K11-Ub_2 and the other Ub_2 chains. Taken together, our data show that K11-linked polyUb chains possess structural and functional properties different from both K48-linked and K63-linked chains. These results support the general hypothesis that differentially linked polyUbs interact with Ub-binding proteins via different binding modes (Fushman and Wilkinson, 2011).

It should be pointed out that K11-Ub_2 interacts with proteasome-associated shuttle proteins specifically. This is an important finding as the structural basis for proteasomal recognition of K11-linked chains is not yet known. We found that the UBA2 domain from a proteasomal shuttle hHR23a recognizes K11-linked chains with affinity intermediate between those for K48-linked and K63-linked chains. By contrast, the linkage-nonselective UBA from another shuttle protein, UQ1, bound to K11-Ub_2 tightly and with similar affinities as for K48-linked and K63-linked chains. We speculate that in order for substrates tagged with K11-linked polyUb to be degraded efficiently by the proteasome, there either exists a yet unidentified K11-specific proteasomal receptor or the lifetime of K11-linked chains at the proteasome is increased relative to K48-linked chains to compensate for the weaker affinity between UBA2 and K11-linked chains.

Together with the ubiquitination machinery, deubiquitinating enzymes (DUBs) regulate the homeostasis of polyUb chains and maintain the pool of free Ub in the cell (Glickman and Adir, 2004). Many USP family DUBs (USP2, USP5, USP15) show little preference for linkage and cleave K11 linkage virtually identically to the canonical K48 and K63 linkages (Bremm and Komander, 2011). That ubiquitination with K11-linked chains can target proteins for proteasomal degradation (Matsumoto et al., 2010; Wickliffe et al., 2011a), and the finding (above) that the UBA domains of proteasomal shuttle proteins have affinity for K11-Ub_2, implies that these chains are translocated to the proteasome. This also suggests that there should be a mechanism for disassembly of K11-linked polyUb at the proteasome. Indeed, our preliminary data (Figure S13) indicate that the proteasome-associated DUB Ubp6 (USP14 in humans) does disassemble K11 linkages, albeit slower than K48 linkages but faster than K63 linkages. This suggests that the proteasome possesses the machinery necessary to process K11 linkages and, from a mechanistic perspective, that the proteasome has a means to control the rate of disassembly of different linkages. The latter also suggests that once translocated to the proteasome, K11-linked polyUb would have an intermediate residency time between K48- and K63-linked chains before getting disassembled.

Much work remains to be done in elucidating the relationship between structural and dynamical properties of polyUb chains and their biological function. The studies presented herein revealed unique structural and dynamical properties of K11-linked chains. The versatility of K11-linked chains as a molecular signal is highlighted by the range of conformations observed and the different pathways in which K11-linked chains are involved. Understanding their signaling function will require identification of their designated receptors and elucidation of the role of interdomain motions in the recognition processes.

EXPERIMENTAL PROCEDURES

Protein Expression and Enzymatic Synthesis of K11-Ub_2

Ub monomers were expressed and purified as described in Varadan et al., 2004; hHR23A UBA2 as in Varadan et al., 2004; UQ1-UBA as in Zhang et al., 2008; and Rap80 tUIM as in Sims and Cohen, 2009. PolyUb chains were made using controlled-length chain assembly (Pickart and Raasi, 2005) combined with domain-specific isotope labeling (Varadan et al., 2002).

NMR Spectroscopy

All NMR experiments were performed at 23°C on a 600 MHz spectrometer equipped with a cryoprobe. Unless otherwise noted, samples of K11-Ub_2 were prepared at pH 6.8 with 20 mM sodium phosphate buffer, 0.02% NaN_3, and 7% D_2O. CSPs were quantitated as follows:

$$\Delta\delta = \left[(\Delta\delta_H)^2 + \left(\frac{\Delta\delta_N}{5}\right)^2\right]^{1/2}, \quad (1)$$

where $\Delta\delta_H$ and $\Delta\delta_N$ are the differences in the chemical shift for ^1H and ^{15}N, respectively, between a Ub unit in Ub_2 and the corresponding Ub monomer.

^{15}N Relaxation Measurements

The ^{15}N longitudinal (R_1) and transverse (R_2) relaxation rates and $\{^1H\}$-^{15}N steady-state nuclear Overhauser enhancement (hetNOE) were measured using samples of K11-Ub_2 (125 μM) with each Ub ^{15}N-enriched separately. The ratio ρ of ^{15}N relaxation rates was calculated as in Fushman et al., 1999, 2004:

$$\rho = \left(2\frac{R_2'}{R_1'} - 1\right)^{-1} \quad (2)$$

RDC measurements and alignment tensor determination are detailed in Supplemental Information.

MTSL Spin Labeling

The paramagnetic spin label 1-oxyl-2,2,5,5-tetramethyl-3-pyrroline-3-methyl methanesulfonate (MTSL) was attached to a Cys at position 36, introduced via site-directed mutagenesis. The PRE effects were quantitated as the ratio (I/I_0) of the signal intensities in the HSQC spectra recorded with MTSL in the oxidized and reduced states. The location of the spin label was determined using SLFIT (Ryabov and Fushman, 2006).

SANS Measurements

SANS measurements were performed on the NG3 30-m SANS instrument (Glinka et al., 1998) at the NIST Center for Neutron Research (NCNR) in Gaithersburg, MD.

Binding Studies

Starting concentrations of ^{15}N-labeled Ub_2 were around 100–125 μM. Stock ligand concentrations generally ranged from 3 mM to 6 mM. Binding was monitored using ^1H-^{15}N SOFAST-HMQC spectra as a function of ligand concentration. CSPs were quantitated using Equation 1, where Δδ is the chemical shift difference between the bound and free species.

Further details on the experimental procedures are in Supplemental Information.

SUPPLEMENTAL INFORMATION

Supplemental Information includes Supplemental Experimental Procedures, 13 figures, and 3 tables and can be found with this article online at http://dx.doi.org/10.1016/j.str.2013.04.029.

ACKNOWLEDGMENTS

We thank M. Rape for providing us with Ube2S plasmid, R.E. Cohen for Rap80 tUIM plasmid, M.H. Glickman for Ubp6 plasmid, and A. Storaska for collecting preliminary data on Rap80 binding to K48-Ub_2 and K63-Ub_2. This work was funded by an NSF postdoctoral award to C.A.C. and NIH grants GM065334 and GM095755 to D.F. and utilized facilities supported in part by the NSF under Agreement No. DMR-0944772.

Received: December 26, 2012
Revised: April 5, 2013
Accepted: April 26, 2013
Published: July 2, 2013

REFERENCES

Beal, R., Deveraux, Q., Xia, G., Rechsteiner, M., and Pickart, C. (1996). Surface hydrophobic residues of multiubiquitin chains essential for proteolytic targeting. Proc. Natl. Acad. Sci. USA *93*, 861–866.

Berlin, K., O'Leary, D.P., and Fushman, D. (2010). Structural assembly of molecular complexes based on residual dipolar couplings. J. Am. Chem. Soc. *132*, 8961–8972.

Bremm, A., and Komander, D. (2011). Emerging roles for Lys11-linked polyubiquitin in cellular regulation. Trends Biochem. Sci. *36*, 355–363.

Bremm, A., Freund, S.M.V., and Komander, D. (2010). Lys11-linked ubiquitin chains adopt compact conformations and are preferentially hydrolyzed by the deubiquitinase Cezanne. Nat. Struct. Mol. Biol. *17*, 939–947.

Castañeda, C.A., Liu, J., Chaturvedi, A., Nowicka, U., Cropp, T.A., and Fushman, D. (2011). Nonenzymatic assembly of natural polyubiquitin chains of any linkage composition and isotopic labeling scheme. J. Am. Chem. Soc. *133*, 17855–17868.

Clore, G.M., and Garrett, D.S. (1999). R-factor, free R, and complete cross-validation for dipolar coupling refinement of NMR structures. J. Am. Chem. Soc. *121*, 9008–9012.

Dynek, J.N., Goncharov, T., Dueber, E.C., Fedorova, A.V., Izrael-Tomasevic, A., Phu, L., Helgason, E., Fairbrother, W.J., Deshayes, K., Kirkpatrick, D.S., and Vucic, D. (2010). c-IAP1 and UbcH5 promote K11-linked polyubiquitination of RIP1 in TNF signalling. EMBO J. *29*, 4198–4209.

Fushman, D., and Wilkinson, K. (2011). Structure and recognition of polyubiquitin chains of different lengths and linkage. F1000 Biology Reports *3*, 10.3410/B3-26.

Fushman, D., Xu, R., and Cowburn, D. (1999). Direct determination of changes of interdomain orientation on ligation: use of the orientational dependence of 15N NMR relaxation in Abl SH(32). Biochemistry *38*, 10225–10230.

Fushman, D., Varadan, R., Assfalg, M., and Walker, O. (2004). Determining domain orientation in macromolecules by using spin-relaxation and residual dipolar coupling measurements. Prog. Nucl. Magn. Reson. Spectrosc. *44*, 189–214.

Ghose, R., Fushman, D., and Cowburn, D. (2001). Determination of the rotational diffusion tensor of macromolecules in solution from NMR relaxation data with a combination of exact and approximate methods—application to the determination of interdomain orientation in multidomain proteins. J. Magn. Reson. *149*, 204–217.

Glickman, M.H., and Adir, N. (2004). The proteasome and the delicate balance between destruction and rescue. PLoS Biol. *2*, E13.

Glinka, C.J., Barker, J.G., Hammouda, B., Krueger, S., Moyer, J.J., and Orts, W.J. (1998). The 30 m Small-Angle Neutron Scattering instruments at the National Institute of Standards and Technology. J. Appl. Cryst. *31*, 430–445.

Iwai, K. (2012). Diverse ubiquitin signaling in NF-κB activation. Trends Cell Biol. *22*, 355–364.

Matsumoto, M.L., Wickliffe, K.E., Dong, K.C., Yu, C., Bosanac, I., Bustos, D., Phu, L., Kirkpatrick, D.S., Hymowitz, S.G., Rape, M., et al. (2010). K11-linked polyubiquitination in cell cycle control revealed by a K11 linkage-specific antibody. Mol. Cell *39*, 477–484.

Mueller, T.D., Kamionka, M., and Feigon, J. (2004). Specificity of the interaction between ubiquitin-associated domains and ubiquitin. J. Biol. Chem. *279*, 11926–11936.

Pickart, C.M., and Raasi, S. (2005). Controlled synthesis of polyubiquitin chains. Methods Enzymol. *399*, 21–36.

Raasi, S., Varadan, R., Fushman, D., and Pickart, C.M. (2005). Diverse polyubiquitin interaction properties of ubiquitin-associated domains. Nat. Struct. Mol. Biol. *12*, 708–714.

Ryabov, Y., and Fushman, D. (2006). Interdomain mobility in di-ubiquitin revealed by NMR. Proteins *63*, 787–796.

Ryu, K.-S., Lee, K.-J., Bae, S.-H., Kim, B.-K., Kim, K.-A., and Choi, B.-S. (2003). Binding surface mapping of intra- and interdomain interactions among hHR23B, ubiquitin, and polyubiquitin binding site 2 of S5a. J. Biol. Chem. *278*, 36621–36627.

Sato, Y., Yoshikawa, A., Mimura, H., Yamashita, M., Yamagata, A., and Fukai, S. (2009). Structural basis for specific recognition of Lys 63-linked polyubiquitin chains by tandem UIMs of RAP80. EMBO J. *28*, 2461–2468.

Sims, J.J., and Cohen, R.E. (2009). Linkage-specific avidity defines the lysine 63-linked polyubiquitin-binding preference of rap80. Mol. Cell *33*, 775–783.

Sokratous, K., Roach, L.V., Channing, D., Strachan, J., Long, J., Searle, M.S., Layfield, R., and Oldham, N.J. (2012). Probing affinity and ubiquitin linkage selectivity of ubiquitin-binding domains using mass spectrometry. J. Am. Chem. Soc. *134*, 6416–6424.

Tolman, J.R., and Ruan, K. (2006). NMR residual dipolar couplings as probes of biomolecular dynamics. Chem. Rev. *106*, 1720–1736.

Varadan, R., Walker, O., Pickart, C., and Fushman, D. (2002). Structural properties of polyubiquitin chains in solution. J. Mol. Biol. *324*, 637–647.

Varadan, R., Assfalg, M., Haririnia, A., Raasi, S., Pickart, C., and Fushman, D. (2004). Solution conformation of Lys63-linked di-ubiquitin chain provides clues to functional diversity of polyubiquitin signaling. J. Biol. Chem. *279*, 7055–7063.

Varadan, R., Assfalg, M., Raasi, S., Pickart, C., and Fushman, D. (2005). Structural determinants for selective recognition of a Lys48-linked polyubiquitin chain by a UBA domain. Mol. Cell *18*, 687–698.

Walker, O., Varadan, R., and Fushman, D. (2004). Efficient and accurate determination of the overall rotational diffusion tensor of a molecule from (15)N relaxation data using computer program ROTDIF. J. Magn. Reson. *168*, 336–345.

Wickliffe, K.E., Williamson, A., Meyer, H.-J., Kelly, A., and Rape, M. (2011a). K11-linked ubiquitin chains as novel regulators of cell division. Trends Cell Biol. *21*, 656–663.

Wickliffe, K.E., Lorenz, S., Wemmer, D.E., Kuriyan, J., and Rape, M. (2011b). The mechanism of linkage-specific ubiquitin chain elongation by a single-subunit E2. Cell *144*, 769–781.

Williamson, A., Wickliffe, K.E., Mellone, B.G., Song, L., Karpen, G.H., and Rape, M. (2009). Identification of a physiological E2 module for the human anaphase-promoting complex. Proc. Natl. Acad. Sci. USA *106*, 18213–18218.

Xu, P., Duong, D.M., Seyfried, N.T., Cheng, D., Xie, Y., Robert, J., Rush, J., Hochstrasser, M., Finley, D., and Peng, J. (2009). Quantitative proteomics reveals the function of unconventional ubiquitin chains in proteasomal degradation. Cell *137*, 133–145.

Zhang, D., Raasi, S., and Fushman, D. (2008). Affinity makes the difference: nonselective interaction of the UBA domain of Ubiquilin-1 with monomeric ubiquitin and polyubiquitin chains. J. Mol. Biol. *377*, 162–180.

